Proceedings of Engineering & Technology -PET Vol 96, pp.168-175 **Advances in Energy Transition and Environmental Impacts**

Modeling heat transfer in unventilated granular silos

Yahia Abdelhamid Lakhdari [#1], Lyes Nasseri [#2], DjamelEddine Ameziani [#3], Rayane Lakroune [#4]

#Laboratory of Multiphase Flows and Porous Media University of Sciences and Technology Houari Boumedienne FGMGP, BP 32 El Alia 16111 Bab Ezzouar, Algiers, Algeria

[1]yahia.lakhdari@ usthb.edu.dz
[2]lyes.nasseri@ usthb.edu.dz
[3]djameleddine.ameziani@ usthb.edu.dz
[4]lakrounerayene@gmail.com

ABSTRACT- In both industrial and agricultural settings, having reliable storage systems is essential. Among these systems, storage silos serve as prominent examples of efficient material management. These large cylindrical structures are designed to hold a wide range of products, such as grains or cement, ensuring their protection and facilitating handling and transportation. However, silos function as more than mere large containers, they preserve the quality of stored materials by shielding them from factors like humidity and pests. This study aims to investigate how external environmental conditions, represented by the Biot number applied at the top of the silo, influence the behavior of the stored grains. Two silo configurations with different aspect ratios are examined to identify potential patterns or differences. The governing equations and corresponding boundary conditions are solved using the finite volume approach. The results section presents and analyzes the thermal and flow behavior of the silo.

***Keywords*— *Unventilated silo, Granular silo, Darcy model, Heat transfer, Porous medium*.**

1. INTRODUCTION

Cereal grains such as wheat, corn, and rice play a crucial role in supplying humans with essential nutrients and energy. To maintain their quality, appropriate storage and transportation practices are necessary. Ensuring proper storage conditions is especially important for preventing silo explosions, which are strongly influenced by moisture and temperature control. Excess humidity can promote mold growth and fermentation, generating heat and raising the likelihood of combustion. Likewise, temperature variations can intensify heat accumulation and heighten explosion risks. Tian et al. [1] used an artificial-aging treatment to evaluate deterioration processes in stored wheat. This accelerated aging approach showed that wheat embryo cells lost clear interstitial spaces, bonding between the endosperm's protein matrix and starch granules weakened, and more starch granules became exposed, with protein fragments appearing on their surfaces. Based on these results, the authors proposed strategies for breeding improved wheat varieties Quemada-Villagómez et al. [2] analyzed how air temperature and moisture interact with sorghum grain inside a silo using yearlong meteorological data. They reported that internal silo temperatures reached up to 42 °C when accounting for heat generated by grain respiration, whereas earlier studies that ignored environmental effects recorded temperatures around 35 °C. Spontaneous ignition commonly occurs when stored materials generate more heat than can dissipate through the silo walls. Ziegler et al. [3], in their review, described existing grain-storage systems, outlined best practice steps for proper maintenance, and summarized major studies aimed at ensuring high quality grain production. Their findings indicate that significant gaps remain in grain storage research, and the review details the features of different storage systems and the recommended operating conditions for each. Hammami et al. [4] proposed a heat and mass balance mathematical model capable of predicting grain temperature and moisture levels to protect grain quality, they also reviewed how airflow characteristics influence moisture and temperature distributions inside silos. Many researchers [5–8] have characterized typical explosion behavior, noting reaction temperatures between 250 °C and 500 °C, CO_2 production, and heavy smoke release. Existing standards [9–11] concerning combustible-dust explosions in silos provide only limited recommendations for prevention and management. Bukrina and Knyazeva [12] introduced a new mathematical model describing the synthesis of intermetallic composites via dynamic thermal explosion, incorporating the chemical-reaction stages. Their results produced the first phase-composition diagrams

ISSN: 1737-9334

Proceedings of Engineering & Technology -PET Vol 96, pp.168-175 **Advances in Energy Transition and Environmental Impacts**

showing how the final product varies with the initial mixture. The study demonstrated that bulk synthesis yields a composite with a complex structure. Himrane et al. [13] numerically analyzed how control parameters affect flow patterns and heat-transfer enhancement in a vertical porous cavity. They identified buoyancy ratio as a key factor shaping three flow modes: chimney flow, reverse flow, and top-aspiration flow. Paola et al. [14] examined explosions triggered by smoldering wood materials and accumulated flammable gases, concluding that appropriate equipment and operational measures are necessary to prevent such events. Allali et al. [15] explored the interaction between natural convection and thermal explosion in porous media, employing Radial Basis Functions for numerical simulation. They observed that a periodic regime arises after the final chaotic stage before conditions evolve toward thermal explosion. Wang et al. [16] numerically examined unsteady periodic natural convection and heat transfer in a square enclosure containing a heated circular cylinder positioned at different heights. Using a temporal spectral method combined with local radial basis functions, they simulated two-dimensional natural convection at Ra = 10^5 with high accuracy. Their results show that both the cylinder's vertical placement and the pulsating temperature strongly affect heat transfer behavior. Most prior investigations have focused on either fully closed or fully open geometries, which do not accurately represent actual grain-storage environments. To address this gap, the present study examines how external climatic influences, represented by the Biot number applied at the silo's top, affect internal grain behavior. The examined silo is closed at the bottom and open at the top to better mirror real storage conditions. Three silo configurations with different aspect ratios, corresponding to varying filling levels, are evaluated to identify significant trends or performance differences. The governing equations and boundary conditions are solved using the finite volume method, and the results describe and analyze the thermal and flow characteristics of the silos.

II. MATERIAL AND METHODS

The physical domain of the silo flow is modeled as a vertical porous cylinder (Fig. 1). The flow inside the cylinder is treated as axisymmetric, which makes a two-dimensional formulation suitable. The porous structure is assumed to be homogeneous, isotropic, and completely saturated with a single phase pure fluid that remains in thermal equilibrium with the solid matrix. The thermophysical properties of the fluid are considered constant, except in the body force term of the momentum equations, where the Boussinesq approximation is applied. In this work, flow through the porous medium is described using the Darcy model.

Assumptions:

- The thermophysical properties of both the solid and fluid phases are taken as constant and evaluated at a mean temperature, with the exception of the fluid density, which follows the Boussinesq approximation.
- The flow is considered axisymmetric and analyzed in two dimensions.
- The porous matrix is treated as rigid, uniform, isotropic, and fully saturated with the working fluid.
- Viscous dissipation is neglected because fluid velocities are sufficiently low.
- Darcy's law is employed to characterize the flow within the porous medium.
- The fluid density varies with temperature, under the condition that the temperature difference satisfies $|\Delta T| < T_0$.

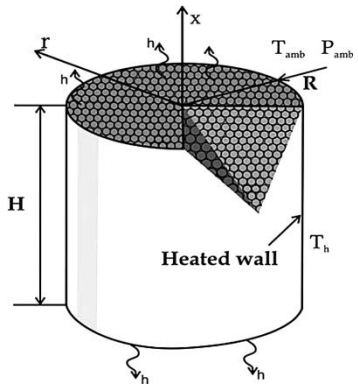

Figure 1: Physical model

The mass conservation equation for an incompressible fluid can be expressed as:

$$\frac{\partial u}{\partial z} + \frac{1}{r}\frac{\partial}{\partial r}(rv) = 0 \#(1)$$

ISSN: 1737-9334

Based on the assumptions outlined earlier, the momentum conservation equation can be written as follows, along the z axis:

$$u = -\frac{k}{\mu}\cdot\frac{dP}{dz} + \frac{k}{\mu}\cdot\rho_0 g\beta(T - T_0) \quad (2)$$

Along axis r

$$v = -\frac{k}{\mu}\cdot\frac{dP}{dr} \quad (3)$$

Replacing equations (2) and (3) in (1): $\rho_0 g\,\beta\,\frac{\partial T}{\partial z} = \frac{\partial^2 P}{\partial z^2} + \frac{1}{r}\left[\frac{\partial}{\partial r}\left(r\frac{\partial P}{\partial r}\right)\right]$ (4)

The energy equation can be expressed as follows::

$$\left(\rho C_p\right)_{eff}\frac{\partial T}{\partial t} + \left(\rho C_p\right)_f\left(u\frac{\partial T}{\partial Z} + v\frac{\partial T}{\partial r}\right) = K_{eff}\left(\frac{\partial^2 T}{\partial Z^2} + \frac{1}{r}\frac{\partial}{\partial r}\left(r\frac{\partial T}{\partial r}\right)\right) \quad (5)$$

The dimensionless form of the mass conservation equation for an incompressible fluid is expressed as:

$$\frac{\partial^2 \mathrm{P}^*}{\partial \mathrm{Z}^{*2}} + \frac{1}{\mathrm{r}^*}\left(\frac{\partial}{\partial \mathrm{r}^*}\left(\mathrm{r}^*\frac{\partial \mathrm{P}^*}{\partial \mathrm{r}^*}\right)\right) = Ra\,\frac{\partial \theta}{\partial \mathrm{z}^*} \quad (6)$$

Where the nondimensional variables are defined as follows:

$(r^*, z^*) = \frac{(r,z)}{\mathrm{H}}$, $(u^*, v^*) = \frac{H}{\alpha_m}(u, v)$, $P^* = \frac{P - P_{atm}}{\Delta P}$, $\theta = \frac{T - T_0}{\Delta T}$ and $t^* = \frac{\alpha_m}{H^2}t$, $\Delta P = \frac{\mu\alpha_m}{K}$, $\Delta T = T_1 - T_0$

The momentum conservation equation is expressed as:

Along axis z

$$\mathrm{u}^* = -\frac{\partial \mathrm{P}^*}{\partial z^*} + Ra\theta \quad (7)$$

Along axis r

$$v^* = -\frac{d\mathrm{P}^*}{dr^*} \quad (8)$$

The dimensionless form of the energy equation is expressed as follows:

$$\sigma\frac{\partial \theta}{\partial \mathrm{t}^*} + \mathrm{u}^*\frac{\partial \theta}{\partial \mathrm{z}^*} + \mathrm{v}^*\frac{\partial \theta}{\partial \mathrm{r}^*} = R_k\left(\frac{\partial^2 \theta}{\partial^2 \mathrm{z}^*} + \frac{1}{\mathrm{r}^*}\frac{\partial}{\partial \mathrm{r}^*}\left(\mathrm{r}^*\frac{\partial \theta}{\partial \mathrm{r}^*}\right)\right) \quad (9)$$

Here, R_k and σ denote the ratios of thermal conductivities and heat capacities, respectively: $\left(R_k = \frac{k_{eff}}{k}, \sigma = \frac{\left(\rho C_p\right)_{eff}}{\left(\rho C_p\right)_f}\right)$. Ra represents the Rayleigh filtration number $\left(Ra = \frac{\rho_0 g\beta\Delta \mathrm{TH}}{\Delta \mathrm{P}}\right)$.

Boundary conditions:

The boundary conditions for this study are defined as follows:

- At the bottom: $\mathrm{U}^*=0$, $\mathrm{V}^*=0$, $\left.\frac{\partial\theta}{\partial z^*}\right|_{(0,r^*,t^*)} = Bi\left(\theta(0, r^*, t^*)\right)$ (10)
- At the top: $\mathrm{P}^*(1, r^*, t^*) = 0$, (if U > 0) $\left.\frac{\partial\theta}{\partial z^*}\right|_{(1,r^*,t^*)} = -Bi\left(\theta(1, r^*, t^*)\right)$, (if U < 0) $\theta(1, r^*, t^*) = 0$ (11)
- Symmetry of the silo: $\left.\frac{\partial \mathrm{P}^*}{\partial r^*}\right|_{(z^*,0,t^*)} = \left.\frac{\partial\theta}{\partial r^*}\right|_{(z^*,0,t^*)} = 0$ (12)
- At the wall: $\left.\frac{\partial \mathrm{P}^*}{\partial r^*}\right|_{(z^*,\mathrm{A},t^*)} = 0$ and $\theta(z^*, \mathrm{A}, t^*) = 1$ (13)

Here, A denotes the aspect ratio, defined as $A = \frac{\mathrm{R}}{\mathrm{H}}$ and $B_i = \frac{hH}{k}$ represents the Biot number, where h is the heat transfer coefficient.

The governing equations along with their boundary conditions are solved using the finite volume method, following the approach outlined by Patankar in 1980 [17]. The solution is considered converged when the error falls below 10^{-6}, using a grid of 81×81 nodes. A fully implicit scheme is employed to ensure numerical stability.

To assess the accuracy of the present study, a comparison (Table 1) was performed based on the heat transfer rate, expressed by the Nusselt number. The results indicate that the maximum relative error remains below 3%.

Table 1: Comparison of Nusselt number results from the present study with those reported by Ameziani et al. [18]

Ra	1	10	100	10^3
Present study	0.676	2.135	6.622	20.501
Ameziani et al. [18]	0.695	2.147	6.637	20.511

ISSN: 1737-9334

Proceedings of Engineering & Technology -PET Vol 96, pp.168-175 **Advances in Energy Transition and Environmental Impacts**

III. RESULTS AND DISCUSSIONS

Figure 2 presents the streamlines within the silo for three Rayleigh numbers ($Ra=10^2$, $Ra=10^3$, $Ra=10^4$ and two Biot numbers (Bi=0.01, Bi=100), with an aspect ratio of A=0.7. The results provide a detailed view of how buoyancy forces and upper boundary thermal conditions influence the internal flow structure.

For all cases, increasing the Rayleigh number leads to a clear intensification of the convective motion. At $Ra=10^2$, the flow remains weak and is characterized by a single, broad convection cell indicative of a regime dominated by conduction. As Ra increases to 10^3, the circulation becomes stronger and more organized, reflecting a transition toward convection driven heat transfer. At Ra= 10^4, the streamlines are highly compressed, indicating vigorous recirculation and a fully developed convective regime. The Biot number affects the flow primarily through the thermal behavior of the upper boundary. When Bi=0.01, the top surface is nearly adiabatic, resulting in relatively smooth and symmetric flow structures. In contrast, for Bi=100, the upper boundary exchanges heat efficiently with the surroundings, producing sharper temperature gradients near the top. This leads to noticeable distortions in the upper region of the convection cell and slightly more intense circulation, particularly at low and moderate Rayleigh numbers. At higher Rayleigh numbers, the internal buoyancy driven dynamics become dominant, reducing the sensitivity of the flow structure to the Biot number. Consequently, for $Ra=10^4$, the overall flow patterns appear similar for both Biot conditions, although localized intensification near the upper boundary remains visible for Bi=100. Overall, the results highlight the interplay between internal buoyancy effects and external thermal boundary conditions. While the Biot number significantly influences the flow at low and moderate Rayleigh numbers, its impact diminishes as convection becomes more dominant.

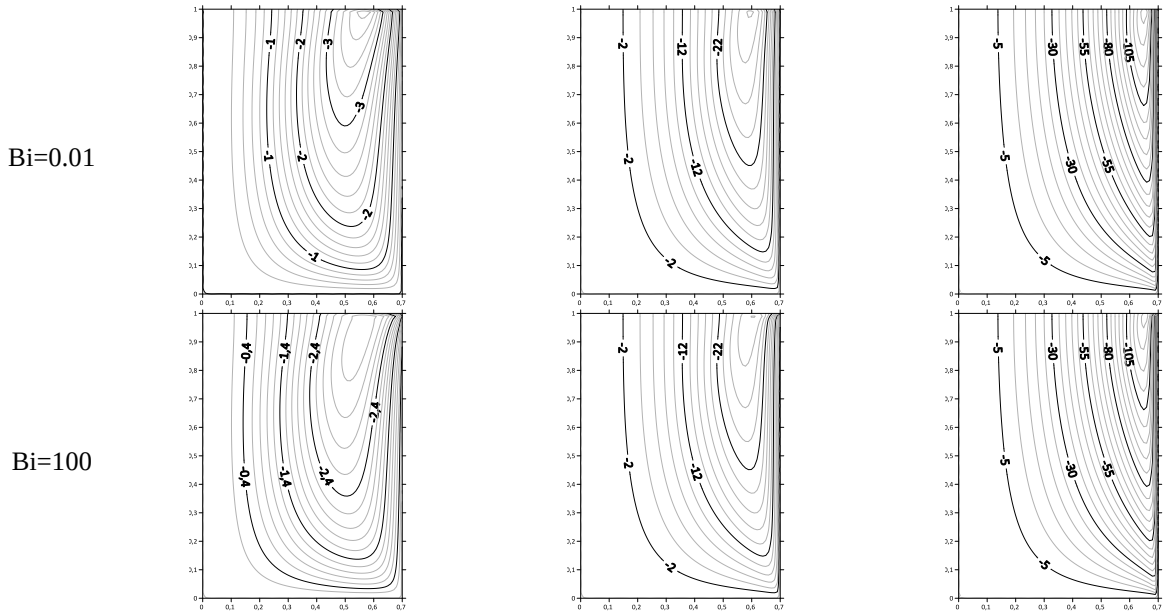

Figure 2: Stream lines as functions of the Rayleigh number for Bi = 0.01&100 and A=0.7.

Figures 3 depict the evolution of isotherm patterns for Bi = 0.01 and Bi = 100, as well as for two filling levels, A = 0.7, over a Rayleigh number range from 10^2 to 10^4. The results highlight the combined influence of wall thermal coupling and geometric confinement on the temperature distribution within the granular domain. For Bi = 0.01, the weakly conductive wall imposes an essentially conduction-dominated regime, with isotherms clustered near the heated boundary regardless of Ra. In contrast, for Bi = 100, the highly conductive wall promotes deeper thermal penetration and enhances internal heat redistribution, particularly when Ra exceeds 10^3, indicating the onset of significant natural convection. Increasing Ra systematically intensifies convective transport: at Ra = 10^2, the thermal field remains conduction like; at Ra = 10^3, the increased spacing and curvature of isotherms reflect improved ventilation; and at Ra = 10^4, a pronounced thermal boundary layer develops along the hot wall, characteristic of fully developed convection. The filling level further modulates these effects. For A = 0.7, the available free space allows larger convective structures to form, amplifying the combined impact of Bi and Ra.

ISSN: 1737-9334

Proceedings of Engineering & Technology -PET Vol 96, pp.168-175 **Advances in Energy Transition and Environmental Impacts**

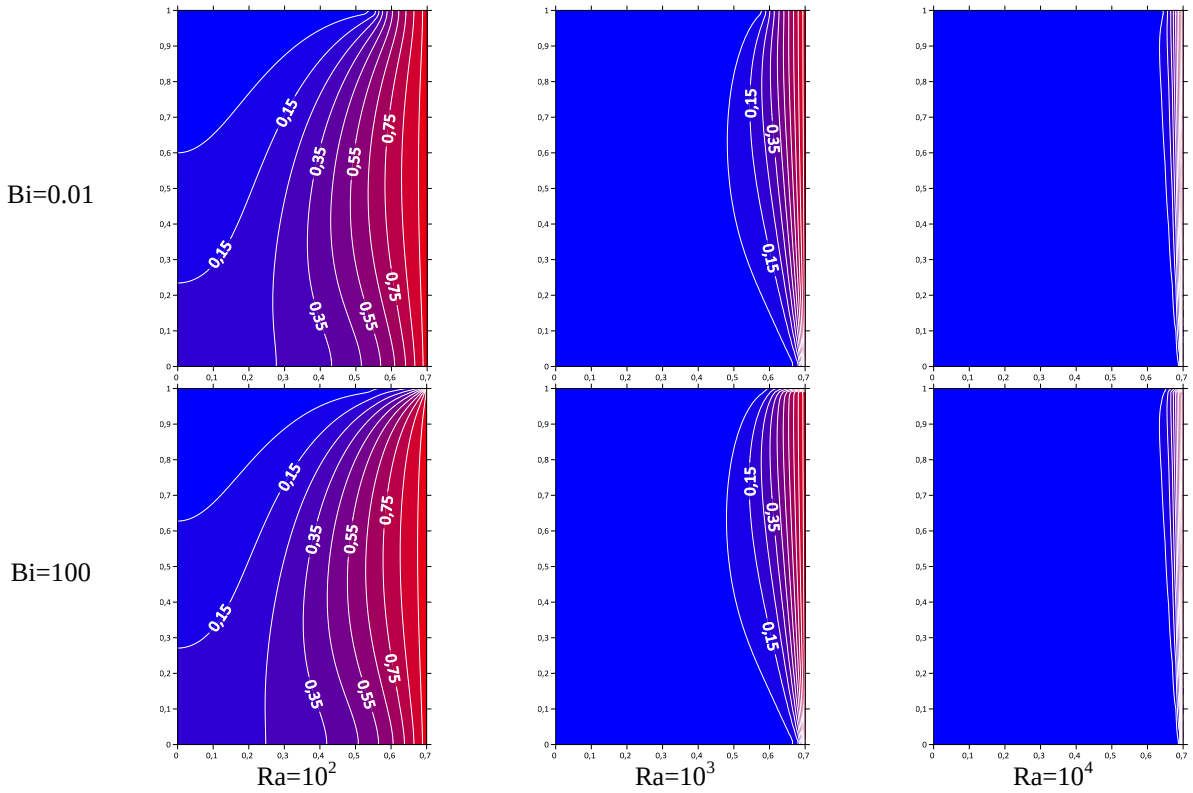

Figure 3: Isotherms as functions of the Rayleigh number for Bi = 0.01& 100 A=0.7.

Figure 4 presents the evolution of the average Nusselt number as a function of the Rayleigh number for two Biot numbers (Bi = 0.01 and 100) and two aspect ratios (A = 0.7 and 0.9). The results clearly indicate that the heat transfer rate increases with the Rayleigh number, reflecting the enhancement of natural convection as buoyancy forces become dominant over conductive effects. For low Rayleigh numbers (Ra $\lesssim$ 10–100), the dependence of Nu on the Biot number is pronounced. In this quasi-conductive regime, the thermal resistance imposed by the boundary conditions governs the global heat transfer, leading to significantly higher Nu values when Bi is large. Beyond a critical Rayleigh number, the differences induced by Bi diminish progressively: the transfer becomes mainly driven by the internal convective motion, and the influence of Bi becomes secondary. The effect of the aspect ratio, examined here for A = 0.7 and 0.9, remains moderate but noticeable, particularly at higher Rayleigh numbers where the flow structure becomes more sensitive to geometric confinement. In general, it is recalled that the most efficient heat transfer configurations correspond to an aspect ratio close to 0.5. At high Rayleigh numbers, all curves tend toward an asymptotic behavior characteristic of fully developed convective regimes. This trend is consistent with order-of-magnitude analyses, leading to a scaling law of the form $Nu \sim Ra^{1/2}$, associated with a thermal boundary layer thickness δ satisfying $Nu \sim 1/\delta$.

ISSN: 1737-9334

Proceedings of Engineering & Technology -PET Vol 96, pp.168-175 **Advances in Energy Transition and Environmental Impacts**

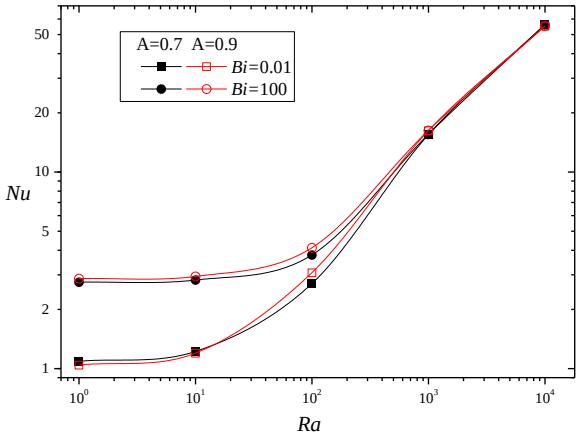

Figure 4: Heat transfer rate as functions of the Rayleigh number for Bi = 0.01, 100 and A=0.7, 0.9.

IV. CONCLUSION

This study has examined heat transfer by natural convection within a vertical cylinder containing a fluid-saturated porous medium, featuring an open outlet at the bottom and a closed top, and subjected to a constant temperature along its sidewall. The flow results reveal a single dominant circulation pattern, characterized by fluid entering through the central region and exiting through the lateral boundary. The principal conclusions can be summarized as follows:

- Enhanced cooling occurs when the stored volume is relatively small (A = 0.7).
- At low Rayleigh numbers, the heat transfer rate increases with both Bi and A.
- For Rayleigh numbers exceeding a critical threshold, buoyancy forces play a stronger role, with their influence remaining dependent on the Biot number.

In perspective, future investigations could focus on tracking chemical reactions within the stored material to gain deeper insight into quality evolution and storage longevity. The development of predictive models incorporating these reactions would further contribute to optimizing storage conditions and improving material preservation.

REFERENCES

[1] P.-P. Tian, Y.-Y. Lv, W.-J. Yuan, S.-B. Zhang, Y.-S. Hu, Effect of artificial aging on wheat quality deterioration during storage, Journal of Stored Products Research, 80 (2019) 50-56.

[2] L.I. Quemada-Villagómez, F.I. Molina-Herrera, M. Carrera-Rodríguez, M. Calderón-Ramírez, G.M. Martínez-González, J.L. Navarrete-Bolaños, H. Jiménez-Islas, Numerical Study to Predict Temperature and Moisture Profiles in Unventilated Grain Silos at Prolonged Time Periods, International Journal of Thermophysics, 41 (2020).

[3] V. Ziegler, R.T. Paraginski, C.D. Ferreira, Grain storage systems and effects of moisture, temperature and time on grain quality - A review, Journal of Stored Products Research, 91 (2021) 101770.

[4] F. Hammami, S. Ben Mabrouk, A. Mami, Modelling and simulation of heat exchange and moisture content in a cereal storage silo, *Mathematical and Computer Modelling of Dynamical Systems*, 22 (2016) 207-220.

[5] U. Krause, Fires in silos, hazards, prevention, and firefighting, *John Wiley & Sons*, 2009.

[6] Eckhoff, Rolf. (2013). Explosion hazards in the process industries. *Explosion Hazards in the Process Industrie*s. 67. 1-439. 10.1016/j.jlp.2020.104225.

[7] A. Clark, J. Kimball, H. Stambaugh, The Hazards Associated with Agricultural Silo Fires, *Federal Emergency Management Agency*, United States Fire Administration, 1998.

[8] R.A. Ogle, S.E. Dillon, M. Fecke, Explosion from a smoldering silo fire, *Process Safety Progress*, 33 (2014) 94-103.

[9] F. Ferrero, C. Lohrer, B.M. Schmidt, M. Noll, M. Malow, A mathematical model to predict the heating-up of large-scale wood piles, *Journal of Loss Prevention in the Process Industries*, 22 (2009) 439-448.

[10] B. Standard, Dust explosion venting protective systems, (2008).

[11] Eckhoff RK. Dust Explosions in the Process Industries: Identification, Assessment and Control of Dust Hazards: *Elsevier Science*; 2003.

[12] N.V. Bukrina, A.G. Knyazeva, The effect of the stages of chemical reactions on the composition of the products formed under a dynamic thermal explosion of the mixtures of aluminium and nickel powders, International Communications in Heat and Mass Transfer, 127 (2021) 105489.

ISSN: 1737-9334

Proceedings of Engineering & Technology -PET Vol 96, pp.168-175 **Advances in Energy Transition and Environmental Impacts**

[13] N. Himrane, D. Ameziani, M. El Ganaoui, H. Ragueb, Some Insights on Unsteady Double Diffusive Natural Convection of Porous Medium in Vertical Open-Ended Cylinder, Arabian Journal for Science and Engineering, 44 (2019) 1379-1392.
[14] P. Russo, A. De Rosa, M. Mazzaro, Silo explosion from smoldering combustion: A case study, *The Canadian Journal of Chemical Engineering*, 95 (2017) 1721-1729.
[15] K. Allali, Y. Joundy, A. Taik, V. Volpert, Dynamics of Convective Thermal Explosion in Porous Media, International Journal of Bifurcation and Chaos, 30 (2020) 2050081.
[16] Z. Wang, T. Wang, G. Xi, Z. Huang, Periodic unsteady natural convection in square enclosure induced by inner circular cylinder with different vertical locations, International Communications in Heat and Mass Transfer, 124 (2021) 105250.
[17] S. Patankar, Numerical heat transfer and fluid flow, *CRC press*, 2018.
[18] Ameziani DE, Bouhadef K, Bennacer R, Rahli O, Analysis of the Chimney Natural Convection in a Vertical Porous Cylinder. *Numerical Heat Transfer, Part A: Applications*. 2008;54(1):47-66.

ISSN: 1737-9334